Journal of Power Sources 196 (2011) 10576–10583

Contents lists available at SciVerse ScienceDirect

Journal of Power Sources

journal homepage: www.elsevier.com/locate/jpowsour

Electrochemical impedance measurements for evaluation of the different components of a complete solid oxide fuel cell associating $La_{0.58}Sr_{0.4}Co_{0.2}Fe_{0.8}O_{3-\delta}$ as cathode, $BaIn_{0.3}Ti_{0.7}O_{2.85}$ as electrolyte and $BaIn_{0.3}Ti_{0.7}O_{2.85}$–Ni cermet as anode

A. Le Gal La Salle*, M. Letilly, E. Quarez, M. Caldes, O. Joubert

Institut des Matériaux Jean Rouxel (IMN), Université de Nantes, Nantes 44322, France

ARTICLE INFO

Article history:
Received 28 April 2011
Received in revised form 24 August 2011
Accepted 27 August 2011
Available online 2 September 2011

Keywords:
Solid oxide fuel cell
Impedance spectroscopy
Fuel cell testing
New electrolyte material

ABSTRACT

It has been demonstrated that $BaIn_{0.3}Ti_{0.7}O_{2.85}$ (BIT07) can be used as electrolyte material in complete intermediate temperature solid oxide fuel cells (IT SOFC), associated with LSCF as cathode material and BIT07–Ni cermet as anode material. Based on those materials, button cells ($\varnothing$ = 10 mm) have been designed. Using electrochemical measurements, the resistance of each part of the complete cell has been minimized, and the optimization of the complete fuel cell has been achieved. A maximum power density of about 266 mW cm^{-2} at 700 °C under wet H_2 on the anode side and air on the cathode one has been reached, with a total area specific resistance of about 0.87 Ω cm^2 at 700 °C. Using impedance measurements, the total resistance of the cell has been decomposed in several parts, attributed to the different components of the cell.

1. Introduction

Solid oxide fuel cells are all-solid devices converting the chemical energy of gaseous fuels, such as hydrogen or natural gas, into electricity via electrochemical processes and presenting advantages such as high energy conversion efficiency, low greenhouse gas emission, or flexibility of fuels [1]. Their operation involves numerous reactions, such as electronic exchanges or diffusion phenomena, arising in the three components of the cell: the anode, the cathode and the electrolyte, and localized either in the bulk of the materials or at the interfaces. Even if the relevant parameter is the global response of the cell in terms of voltage/current and electrical power, it is necessary to characterize the different components separately in order to find the parameters influencing the numerous reactions involved during the cell operation and to identify those limiting the performances of the cell. Impedance spectroscopy is an appropriate method to determine and evaluate the different contributions [2,3].

Due to its intrinsic properties, such as its conductivity level at 700 °C, its stability under a large oxygen partial pressure range and its stability under CO_2 atmosphere, it has been demonstrated in previous published papers that $BaIn_{0.3}Ti_{0.7}O_{2.85}$ (BIT07) is a suitable electrolyte material for SOFC [4,5]. It has been demonstrated that this material can be used with well-known cathode materials, such as $La_{0.7}Sr_{0.3}MnO_{3-\delta}$ (LSM), $La_{0.58}Sr_{0.4}Co_{0.2}Fe_{0.8}O_{3-\delta}$ (LSCF) or $Nd_2NiO_{4+\delta}$, and that best results have been obtained with LSCF [6], probably due to the self-induced formation of an accommodating layer of formula $Ba_xLa_{0.58(1-x)}Sr_{0.4(1-x)}In_{0.3x}Ti_{0.7x}Co_{0.2(1-x)}Fe_{0.8(1-x)}O_{3-\delta}$, with $0 \leq x \leq 1$, and x increasing continuously from 0 to 1 when going from the BIT07 electrolyte side to the LSCF cathode [7]. It has been shown that this layer is not resistive, in contrary to what is observed between LSCF and the usual YSZ electrolyte [8–10], and allows an excellent match between the electrolyte and cathode, with mechanical and electrochemical properties varying continuously from the electrolyte and cathode, as it is the case of graded or multi-layered electrodes [11,12] and avoiding thermal expansion coefficient mismatch between cathode and electrolyte [13–15]. By screen-printing LSCF onto BIT07 dense pellets and performing an appropriate heat treatment, it is possible to obtain reproducible LSCF/BIT07/LSCF symmetrical cells with interesting electrochemical properties such an ASR value of 0.07 Ω cm^2 [14].

It has been first published that a dense electrolyte could be prepared with a powder synthesised by solid-state reaction, ball-milled in order to reduce the grain size and finally sintered at 1300 °C [16]. BIT07 can also be used in a cermet anode combined with nickel since neither Ni nor NiO react with BIT07. Symmetrical anode/electrolyte/anode cells have thus been prepared by tape casting and co-firing. By varying the grain size of BIT07 powders, the BIT07/NiO ratio, the use of some pore-forming agents, numerous anode compositions have been tested, and a minimal ASR value of 0.15 Ω cm^2 was finally obtained at 700 °C under wet (3% H_2O)

* Corresponding author. Tel.: +33 2 40 37 39 13; fax: +33 2 40 37 39 95.
E-mail address: Annie.Legal@cnrs-imn.fr (A. Le Gal La Salle).

0378-7753/$ – see front matter © 2011 Elsevier B.V. All rights reserved.
doi:10.1016/j.jpowsour.2011.08.108

Ar/H_2 (95/5) atmosphere for a cermet anode composed of BIT07 and NiO in a 50:50 weight ratio, and 5 wt.% carbon black [17].

Finally, complete LSCF/BIT07/BIT07–Ni cells have been realized, and tested under air on the cathode side and wet H_2 (3% H_2O) on the anode side [16]. Good performance have been reached but discussed only in terms of total polarization resistance determined from current density/voltage curve (J/U) at the open circuit voltage (OCV). The aim of this paper is to use impedance measurements to understand the origin of this resistance, and to determine the relevant parameters that can be modified in order to minimize it.

2. Experimental

2.1. Powders

BIT07 was synthesised as detailed in [5]: its constituents, high purity barium carbonate (Alfa Aesar), indium oxide (Alfa Aesar) and titanium dioxide (Merck), in stoichiometric ratio, were mixed in mortar and pestle using alcohol. The mixture was first heated at 1200 °C for 24 h, then ground and compacted into a pellet of 40 mm diameter. This compact was then heated at 1350 °C for 24 h, ground and passed through mesh 100.

LSCF powder was provided by Marion Technologie and nickel oxide powder (grain size 0.5–1 μm) was provided by Pharmacie Centrale de France.

The purity of the powders was checked by X-ray powder diffraction (XRPD) recorded at room temperature, in Bragg–Brentano reflection geometry using a Brüker "D8 Advance" powder diffractometer with a Cu anode as X-ray source and equipped with the Vαrio1, a Johansson type Germanium (1 1 1) monochromator that provides pure Kα1 radiation ($\lambda = 1.54056$ Å, $20° < 2\theta < 90°$, step = 0.02°) and a 1-D position-sensitive detector (Vantec).

2.2. Preparation of BIT07 pellets

Samples used for impedance measurements were obtained by compacting BIT07 powder into pellets. After synthesis, the grain size of the BIT07 powder, measured with a Coulter LS230 instrument, shows a large extend between 0.6 and 60 μm, with 60% of particles with grain size in the 3–12 μm range. After compacting into pellets and sintering at 1350 °C for 24 h, the corresponding relative density of the sample is of 80%. In order to obtain dense samples, BIT07 raw powder has been ball milled in 45 ml silicon nitride pot with 15 silicon nitride balls in ethanol at 500 rpm using FRITSCH P7 planetary micro mill before sintering. When ball-milling for 2 h [18] and sintering at 1350 °C for 24 h, the relative density reaches 91% (grain size of 3 μm), whereas ball-milling for 60 h and sintering at 1300 °C for 9 h leads to particles of about one micron or less and to a density value of 95%.

2.3. Preparation of symmetrical LSCF/BIT07/LSCF assemblies

Electrolyte supported symmetrical LSCF/BIT07/LSCF cells have been realized by screen printing (DEK 248) LSCF ink on a BIT07 pellet as described above. The ink was firstly prepared by mixing 60% of LSCF with 40% of a mixture prepared with terpineol 95% and ethyl cellulose 5% (all percentages are weight ratio percentages). The ink is deposited through a circular mask (diameter 8 mm). Four successive ink deposits were done, with an intermediate heating at 120 °C. The LSCF/BIT07 half cell is then heated at 120 °C for 15 min before doing the same deposits on the other side of the pellet. The symmetrical cells are finally sintered 6 h at 1050 °C. This treatment leads to a total cathode deposits thickness of about 20 μm.

2.4. Preparation of symmetrical BIT07–Ni/BIT07/BIT07–Ni assemblies

Both the anode and the electrolyte were prepared by tape casting. First, the electrolyte slurry is prepared by mixing the ball milled BIT07 powder, a dispersant (oleic acid) and an azeotropic mixture of solvents (ethanol and 2-butanon) in 45 ml silicon nitride pot with 12 silicon nitride balls at 240 rpm using FRITSCH planetary micro mill P7, for 1 h. Binders (Polyvinyl Butyral PVB-90 and PVB-98) and plasticizers (Polyethylene glycol PEG-400 and dibutyl phthalate) are subsequently added to the former preparation and ball-milled for 24 h at 180 rpm. The slurry constituents' ratios depend on the powder grain size.

Second, the anode slurry is prepared by mixing NiO powder with the previous electrolyte slurry in different BIT07:NiO weight ratio ranging from 30:70 to 50:50. PMMA (methyl polymethacrylate acrylone 4510 from APSA) or carbon black (super P from Timcal) were added (2.5–15 wt.% of the powder amount) to obtain porous anode material.

Half cells are obtained by tape casting a thin electrolyte layer on a thick tape of anode. A sandwich of two previous half cells (anode/electrolyte–electrolyte/anode) gives one symmetrical cell. The cohesion at the electrolyte–electrolyte interface is obtained by co-pressing the assembly.

Finally the following thermal treatment is applied to remove slowly the organic species and to sinter the half-cell:

$$\mathrm{RT} \overset{50\,\mathrm{K\,h^{-1}}}{\longrightarrow} 600\,^{\circ}\mathrm{C}\,(4\,\mathrm{h}) \overset{100\,\mathrm{K\,h^{-1}}}{\longrightarrow} 1300\,^{\circ}\mathrm{C}\,(9\,\mathrm{h}) \overset{100\,\mathrm{K\,h^{-1}}}{\longrightarrow} \mathrm{RT}$$

After sintering, an "anode" supported symmetrical cell is obtained with 100–150 μm thick anode and 20–50 μm thin electrolyte. The surface is comprised between 0.35 and 0.5 cm^2.

2.5. Preparation of complete BIT07–Ni/BIT07/LSCF cells

Anode supported button cells (⌀ 10 mm) were realized by using sintered electrolyte/anode half-cell, as described above where the electrolyte and the anode thicknesses are of about 20 μm and 350 μm respectively. Then a LSCF cathode was deposited on the electrolyte by screen-printing (c.f. Section 2.3) and sintered. Its final diameter is of about 5 mm and its thickness of 20 μm. Gold grids are placed on the two electrodes, with gold ink, as collectors (wire diameter 60 μm, grid opening 250 μm) and the complete cell is treated at 130 °C for one night to evaporate the solvents contained in the gold ink and to obtain good electrical contacts.

2.6. Microscopy studies

The morphology of the different compounds and the quality of the electrode/BIT07 interfaces have been observed by scanning electron spectroscopy performed on a JEOL 6400 apparatus.

2.7. Electrochemical measurements

The impedance diagrams were obtained from a frequency response analyser Solartron 1260 between 250 °C and 700 °C, each 50 °C, after a stabilisation duration of 60 min. Each spectrum has been recorded at $U_{DC} = 0$ V, with a signal amplitude optimized for each studied sample in order to be small enough to meet the linearity requirement of the transfer function, but high enough to have a good signal/noise ratio [3]. The spectrum is realized with 84 points scattered in a frequency range from 2 MHz to 0.01 Hz.

All symmetrical cells described previously have been studied between two gold grids as collectors (wire diameter 60 μm, grid opening 250 μm). In order to check the influence of the nature of the collector some experiments have been realized between platinum

grids collectors. In order to characterize BIT07, electrolyte symmetrical cells where both sides of the BIT07 pellets were coated with Pt or Au paste acting as electrodes have been also studied.

Electrolyte supported cells (with LSCF, Au and Pt electrodes) have been tested under air, whereas anode supported cells (BIT07–Ni/BIT07/BIT07–Ni) have been tested under wet (3%) Ar/H_2 (95/5) atmosphere, after a previous reduction stage at 700 °C for 5 h under the same reducing atmosphere.

The current–voltage (*J–U*) characteristic of the complete cell is measured with the use of a laboratory-made testing system [18]. The button cell was sealed (Aremco sealing material #571) on the top of an alumina sample tube (outer ⌀ 10 mm, inner ⌀ 6 mm) thus separating the atmospheres between the inside and outside of tube, and the system has been optimized in order to minimize gas leak and obtain reproducible voltage and current measurements [5]. The fuel–gas supply tube is situated inside the sample tube. The system was kept vertically in a tubular furnace. Measurements of current and voltage were done by digital multimeters Keithley 197 and Protek 506, respectively. Current drawn in the circuit was varied using a rheostat. Effective area of the cells in this study was 0.2 cm^2 (cathode surface).

3. Results and discussion

3.1. Linearity and precision of measurements

In order to determine the optimal amplitude of the applied perturbation, which has to be small enough to meet the linearity requirement of the transfer function, and sufficiently high to lead to a good signal/noise ratio, several amplitude values have been tried on the three assemblies, and the optimal value has been determined for each of them.

3.1.1. Electrolyte

Three values of amplitude have been tested: 100 mV, 500 mV and 1000 mV) in the 200–700 °C range. All diagrams obtained at each temperature are perfectly superimposed, demonstrating that in this case the linearity requirement is fulfilled, and the value of 1000 mV was retained for following studies.

3.1.2. Cathode/electrolyte/cathode assembly

The Nyquist diagrams do not depend on voltage amplitudes of 10, 30 and 100 mV demonstrating that in this case the linearity requirement is fulfilled. Moreover, all resistance values are comprised in the 0.19–0.21 Ω cm^2 range, allowing to give a precision of the measurement of 0.02 Ω cm^2. For amplitude values superior to 200 mV, the diagrams becomes dependant on the perturbation amplitude and, as expected [19], the resistances increase.

To study if an applied alternative voltage higher than 100 mV has damaged the sample, three successive impedance diagrams have been recorded successively at 10 mV, 1000 mV and 10 mV. The last diagram showing a higher polarisation resistance than the first one, this suggests that a too high voltage amplitude induces a deterioration of the cathode properties [19,20]. In order to obtain diagrams with the best signal/noise ratio, but with the fulfilment of the linearity requirement, the value of 100 mV was finally chosen for all measurements. This value is similar with the ones used in comparable studies [21].

In order to control if the nature of the current collector has an influence on our measurement, impedance diagrams have been successively studied with platinum and gold collectors. The same Nyquist diagrams have been obtained in the two cases, demonstrating that the impedance diagrams are really characteristic of the LSCF/BIT07/LSCF half cells.

3.1.3. Anode/electrolyte/anode assembly

Diagrams plotted with voltage amplitudes smaller or equal to 50 mV are superimposed, demonstrating that in this case the linearity requirement is fulfilled, and the precision of our measurements is in this case of 0.02 Ω cm^2. As it was observed for the cathode, the measurement performed with a 100 mV voltage amplitude has also damaged the sample. In order to obtain diagrams with the best signal/noise ratio, but with the fulfilment of the linearity requirement, the value of 50 mV was finally chosen for all measurements.

3.2. Impedance characterization of the BIT07 electrolyte

3.2.1. Interpretation of impedance measurement on BIT07 pellets

The Nyquist diagram of a BIT07 (density of 95%) pellet recorded at 255 °C under air (with gold collectors) is mainly composed of a depressed semi-circle, which can be modelled by a R//CPE circuit. The expression of the impedance of the CPE (Constant Phase Element), which often characterize inhomogeneous materials, is $1/Q(j\omega)^n$, with an associated capacitance *C* calculated from the formula $(RC)^n = RQ$ [22,23]. In the case of BIT07 it is of about 10^{-11} F cm^{-2}, similar capacitance values have been obtained for layers of the widely used yttria-stabilized zirconia (YSZ) electrolyte [24,25], or cerium oxide based electrolytes [26] suggesting that this contribution is representative of an electrolyte response. The same experiment has been done with platinum instead of gold electrodes, or with LSCF electrodes intercalated between BIT07 electrolyte and gold collectors. In all cases the same semi-circle has been obtained, and is different from the LSCF (*vide infra*) or collector response [27], confirming that it is really characteristic of the BIT07 electrolyte.

When the temperature increases, the size of the semi-circle decreases and at 700 °C, this contribution is only represented by a series resistance Rs because of the frequency shift, associated with a series inductance *L*, the remaining part of the diagram being characteristic of the current collection. The inductance of the set-up is always comprised in the 0.9×10^{-6}–1.1×10^{-6} H range, in accordance with literature concerning similar measurements [28–31].

3.2.2. Determination of BIT07 conductivity

At each temperature, it is possible to calculate the conductivity using the following formula $\sigma = e/(SR)$, where *e* is the thickness of the electrolyte, *S* is the surface area of the electrode and *R* is the resistance extracted from the impedance diagram. The conductivity σ increases when the temperature *T* increases, according to the Arrhenius law (Fig. 1):

$$\sigma = \sigma_0 \exp\left(-\frac{Ea}{kT}\right)$$

As shown in Fig. 1, the conductivity increases together with the observed pellet's density, and the activation energy Ea decreases when the density increases.

When repeating experiments at 700 °C, all Rs resistance values were in a very small range, allowing to give a precision of our conductivity measurements of 0.01×10^{-2} S cm^{-1}. It has also to be noted that in our experimental conditions it was not possible to separate bulk and grain boundary contributions.

3.3. Impedance characterization of the LSCF/BIT07/LSCF symmetrical cell

3.3.1. Interpretation of the electrochemical measurement

The impedance diagram of symmetrical cells LSCF/BIT07/LSCF has been recorded at different temperatures. Below 310 °C, the diagrams present mainly a depressed arc, which can be modelled by a R//CPE circuit where C is of 10^{-11} F cm^{-2}. This value suggests

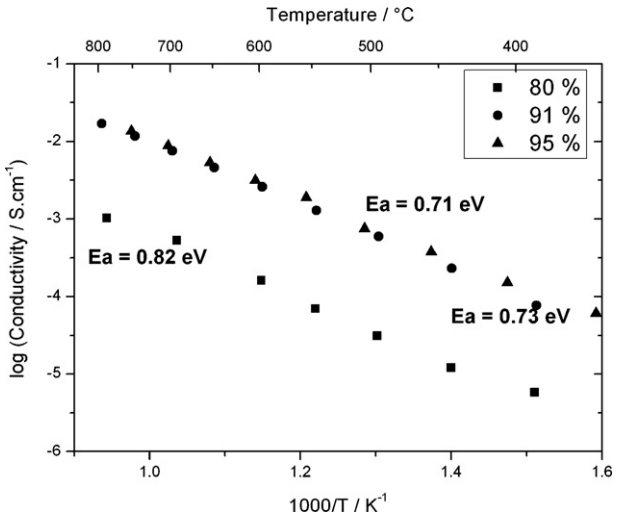

Fig. 1. Variations of the conductivity of BIT07 with temperature for compacity values of 80% (■), 91% (●) and 95% (▲).

that at low temperature the impedance diagrams show mainly the contribution of the electrolyte (see Section 3.2.1).

At higher temperatures, because of the frequency shift, the electrolyte contribution is only represented by a series resistance Rs associated with the series inductance *L*, and the contribution of the cathode can be seen. In air atmosphere (pO_2 = 0.21 atm), the Nyquist plot (Fig. 2a) appears as two depressed arcs, called in the following middle frequency (MF) and low frequency (LF) contributions, and can be modelled by two R//CPE circuits.

The impedance diagram obtained by switching the atmosphere to a low oxygen partial pressure (pO_2 = 0.0005 atm) is presented in Fig. 2b. The superimposition of diagrams (a) and (b) (Fig. 2c), shows that the MF contribution remains the same, on the contrary to the LF contribution, which splits into two contributions, leading to the appearance of a third contribution at very low

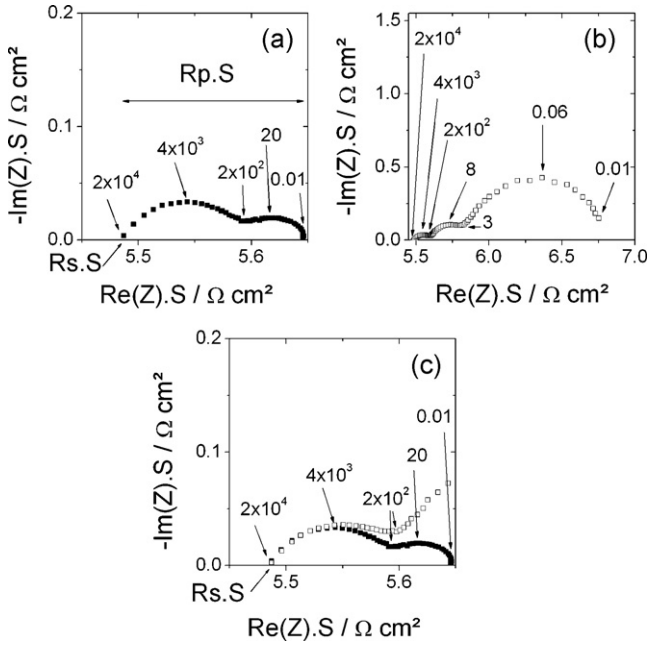

Fig. 2. Nyquist diagram of a symmetrical cell LSCF/BIT07/LSCF measured at U_{DC} = 0 V at 700 °C under air (pO_2 = 0.21 atm) (a) and low pO_2 (0.0005 atm) atmosphere (b). The high frequency parts of these two diagrams are compared in (c). Characteristic frequencies are reported in Hz. Rs and Rp refer to the series resistance and the polarisation resistance respectively.

Table 1
Specific capacity and frequency for the different electrochemical contributions observed on the Nyquist diagram at 700 °C compared to literature data.

	Phenomenon	Capacity (F cm^{-2})	
		This work	Literature data
MF	Charge transfer	10^{-4}	10^{-6}–10^{-3}
LF	Adsorption/diffusion	10^{-1}–10^{-2}	10^{-2}
VLF	Adsorption/diffusion	10^{1}	10^{-1}

frequencies (VLF). Similar observations have already been made for $(La_{1-x}Sr_x)Co_{1-y}Ni_yO_{3-\delta}/Ce_{0.9}Gd_{0.1}O_{1.95}$ [32], LSM–YSZ/YSZ [33], LSM–$Ce_{0.8}Sm_{0.2}O_{1.9}$/YSZ [34] or $La_{0.9}Sr_{0.1}Ga_{0.8}Mg_{0.2}O_{3-\delta}$(LSGM)-$La_{0.6}Sr_{0.4}Co_{0.2}Fe_{0.8}O_{3-\theta}$/LSGM [31] half cells. The LF and the VLF contributions become predominant under very low pO_2 pressure. This result shows that lowering the oxygen concentration leads to a slowing down of the phenomena involved in the low frequency range, confirming that they are correlated to oxygen diffusion. The LF and VLF loops, which are linked to oxygen diffusion, are often modelized by Gerisher-type impedance [31,35,36]. Nevertheless, modelization by R//CPE elements gives also satisfactory results and allows to compare the different materials [32,37–39]. Capacitance values extracted from impedance diagrams are collected in Table 1, and compared to values collected on cells using $(La_{1-x}Sr_x)_sCoO_{3-\delta}$ [32] or LSCF-based materials [40–45] as cathode. The capacity values and the independence of the MF arc on atmosphere allow us to identify this phenomenon as the charge transfer at the electrolyte/cathode interface. Moreover, the MF arc is very depressed, probably reflecting the effect of the graded interface, with the presence of the whole range of compositions between LSCF and BIT07 [14]. The dependence of the LF and VLF loops on atmosphere and the associated capacity values, confirm that they are linked to diffusion phenomena in accordance with literature.

3.3.2. Determination of assembly performance

The area specific resistance (ASR) can be deduced from the polarisation resistance (Rp), which is the sum of R_{MF} and R_{LF} (ASR = Rp · *S*/2, where *S* is the cathode surface and the 2 factor accounts for the fact that the cell is symmetrical). Its thermal evolution (both activation energy which is about 1 eV and the ASR value at 700 °C of 0.08 Ω cm^2,) is in accordance with preliminary results published in [6,7]. Based on the ASR values comparison, the influence of the cathode microstructure on the performances has been investigated [14], and leads to a minimal value of 0.07 Ω cm^2, which competes favorably with best results already published with LSCF-based cathodes [9,36,37,40–43,46].

3.3.3. Ageing experiment

In previous papers [6,7], it has been established that for LSCF at 700 °C, the ASR increases regularly with time. Fig. 3 presents both the impedance diagrams and the micrographs of the LSCF cathode before and after ageing at 700 °C under air. Although a small variation of Rs is also observed during ageing [14], the diagram recorded after ageing has been shifted in order to present the same Rs value as before, allowing an easier comparison of the two loops of the impedance diagram. The figure shows the simultaneous densification of the electrode and the increase of the low frequency resistance, confirming once again the link between this loop and the diffusion phenomena. Nevertheless, ageing phenomena are often quite complex [32], and in the case of our studies are not limited to densification. A more detailed study is presented elsewhere [14].

3.4. Impedance characterization of the Ni–BIT07/BIT07/Ni–BIT07 symmetrical cell

Using various experimental conditions, obtained by varying the grain size of BIT07 powders, the BIT07:NiO ratio and the amount of

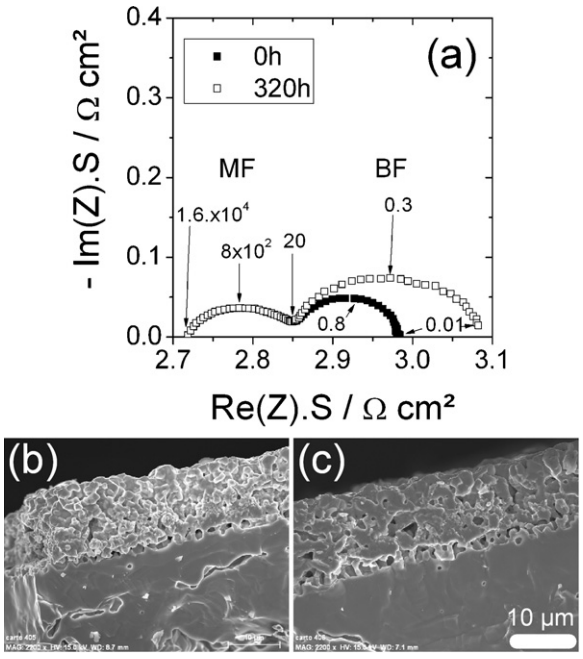

Fig. 3. Comparison of the impedance diagrams at 700 °C at U_{DC} = 0 V under air (a) (characteristic frequencies are reported in Hz) and of the micrographs of the LSCF/BIT07 interface before (b) and after (c) ageing at 700 °C under air.

the pore-forming agents, numerous anode compositions have been tested, and lead to numerous assemblies [16,17] with very different properties, that can be ordered in three categories.

3.4.1. First category

Fig. 4 shows a typical diagram of the samples of the first category. This type of diagrams has been obtained for cermet anodes prepared with a minimal quantity of 40 wt.% of NiO and carbon black as pore-forming agent in quantity comprised between 5 (for 40 wt.% NiO) and 7.5 wt.% (for higher NiO concentration), and presenting a good simultaneous percolation of the three ceramic, metallic and porous networks. The intersection of the high frequency part of the diagram with the real axis leads to a resistance value Rs, which

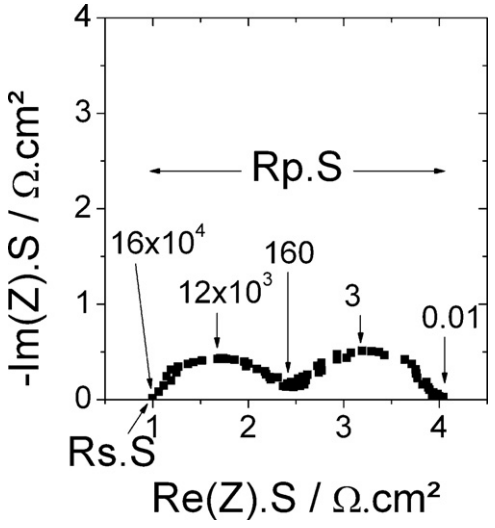

Fig. 4. Nyquist diagram at 700 °C at U_{DC} = 0 V under wet (3%) Ar/H_2 (95/5), of a symmetrical cell BIT07–Ni/BIT07/BIT07–Ni. The BIT07–Ni cermet has been prepared with 40 wt.% of NiO and 5 wt.% of carbon black. Characteristic frequencies are reported in Hz. Rs and Rp refer to the series resistance associated to the electrolyte and the polarisation resistance respectively.

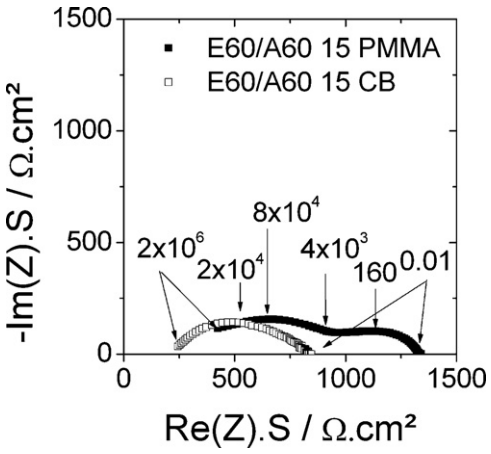

Fig. 5. Nyquist diagram at 700 °C at U_{DC} = 0 V under wet (3%) Ar/H_2 (95/5), of a symmetrical cell BIT07–Ni/BIT07/BIT07–Ni. The BIT07–Ni cermet has been prepared with 40 wt.% of NiO and 15 wt.% of carbon black (□) and PMMA (■). Characteristic frequencies are reported in Hz.

corresponds to the electrolyte contribution. Indeed, the conductivity σ, calculated using the formula $\sigma = e/(S\ \mathrm{Rs})$ (where e is the thickness of the electrolyte, S is the surface area of the electrode and Rs is the resistance extracted from the impedance diagram) is of 0.5×10^{-2} S cm^{-1}, i.e. in good agreement with the usual BIT07 conductivity values (such as these determined in Section 3.2). The diagram presents two contributions, which can be modelled by two R//CPE circuits, with respective capacitance values of 2×10^{-5} and 6×10^{-2} F cm^{-2}. Similar capacitance values have been reported for anode/electrolyte assemblies, realized with YSZ/NiO cermet anode onto YSZ electrolyte [47–49]: the first loop can be associated with charge transfer process and H_2O formation, whereas the second one corresponds to dissociative adsorption and surface diffusion/gas phase diffusion, and associated capacitance values are comparable to the ones observed in our case.

3.4.2. Second category

Fig. 5 shows two diagrams typical of the second category of samples, prepared with PMMA, or with 40 wt.% of NiO and quantities of carbon black comprised between 7.5 and 15 wt.% NiO. These diagrams show mainly two highly resistive phenomena, which can be modelled by two R//CPE circuits with a series resistance Rs.

For all samples of this type, the capacitance values associated to the first phenomenon are comprised between 2×10^{-9} and 15×10^{-9} F cm^{-2}. To our knowledge, such results, with so low capacitances values observed at 700 °C, are not described in literature for anode contributions. Calculating a conductivity, either by using the Rs value, or by adding to Rs the resistance associated to the first R//CPE element, leads in all cases to values smaller than 5×10^{-5} S cm^{-1}, which are not in agreement with the BIT07 conductivity values established in Section 3.2. This result is probably linked to the fact that the Ni–BIT07 electrodes are in these cases so resistive that they hide totally the electrolyte response, contrary to which was observed with gold, platinum or LSCF electrodes.

The second contribution can be modelized by a R//CPE circuit, with capacitance values comprised in the 10^{-6} and 6×10^{-6} F cm^{-2} range, in accordance with charge transfer phenomenon [47–49]. No low frequency contribution, associated to adsorption and surface diffusion/gas phase diffusion as reported for anode/electrolyte assemblies [47–49] is observed. The interpretation of these diagrams is not complete. Nevertheless impedance measurements show that these samples are not suitable for use in a fuel cell, with no simultaneous percolation of the three ceramic, metallic and porous networks. As an example, Fig. 6, which presents the

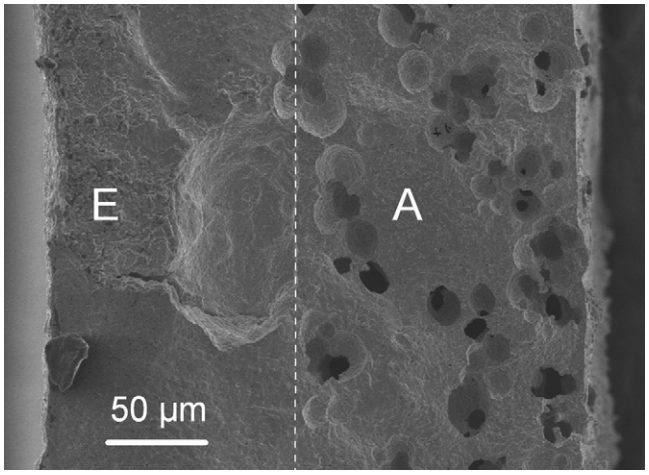

Fig. 6. SEM picture of the BIT07/BIT07–Ni interface, for a BIT07–Ni cermet prepared with 40 wt.% of NiO and 15 wt.% PMMA.

SEM picture of the sample prepared with PMMA, reveals the inhomogeneity of the porosity of this sample, and confirms the result of the electrochemical impedance characterization.

3.4.3. Third category

Fig. 7 shows characteristic of the third category of samples, gathering samples containing high amounts of nickel. The high frequency intersection of the diagram with the real axis leads to resistance corresponding to the usual BIT07 conductivity at 700 °C (Section 3.2). The diagram can be modelized by two R//CPE contributions with respective capacitance values of 6×10^{-6} and 10^2 F cm^{-2} range. If the first value is in good agreement with a classical charge transfer phenomenon [47–49], the second one presents a very high capacitance value suggesting that the diffusion phenomena are strongly modified. In the case of these samples, it has been observed that the ASR measured between the two intersections of the diagram with the real axis decreases when the temperature decreases, that can be explained by the fact that the quantity of carbon black is not enough to assure a percolation of the porosity.

Based on the ASR values comparison, the influence of the anode composition on the performances has been investigated, and leads to a minimal value of 0.15 Ω cm^2 [17].

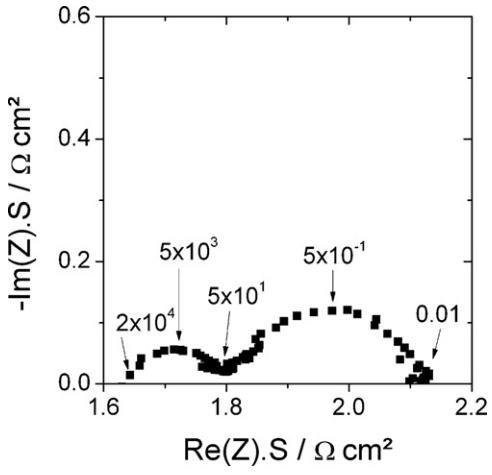

Fig. 7. Nyquist diagram at 700 °C at U_{DC} = 0 V under wet (3%) Ar/H_2 (95/5), of a symmetrical cell BIT07–Ni/BIT07/BIT07–Ni. The BIT07–Ni cermet has been prepared with 50 wt.% of NiO and 2.5 wt.% of carbon black. Characteristic frequencies are reported in Hz.

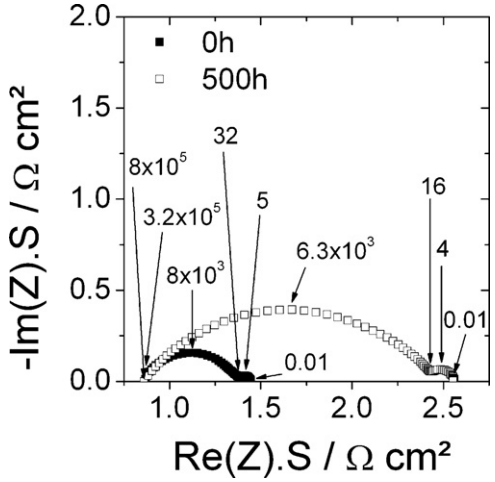

Fig. 8. Comparison of the Nyquist diagrams at 700 °C at U_{DC} = 0 V of a symmetrical cell BIT07–Ni/BIT07/BIT07–Ni before (■) and after (□) ageing at 700 °C under wet (3%) Ar/H_2 (95/5). Characteristic frequencies are reported in Hz.

3.4.4. Ageing experiment

Results detailed in future publication show that at 700 °C under wet (3% H_2O) Ar/H_2 (95/5), the ASR increases regularly with time, with also a small variation of Rs [17]. As shown in Fig. 8, on which the two diagrams have been superimposed (with a shift of the diagram plotted after ageing in order to have the same Rs value than before ageing). In contrary to what was observed for cathode/electrolyte/cathode cells, the modifications induced during ageing concern mainly the MF loop, revealing an important resistance increase of the associated phenomena. SEM and EDX microscopy studies before and after 500 h at 700 °C reveal no apparent modification of the porosity of the electrode, but an aggregation of nickel, as it has been observed for Ni–YSZ ageing [50]. This result is therefore confirmed by impedance measurements, which are in accordance with a slowing of the charge transfer phenomena.

3.5. Electrochemical characterization of the complete LSCF/BIT07/Ni–BIT07 cell

Fig. 9 shows the voltage U and power density versus current density J curves at 700 °C, under air on the cathode side and under wet (3% H_2O) H_2 on the anode side, and the impedance diagram obtained for the total cell under the same measuring conditions at the open circuit voltage. These results compete favorably with comparable laboratory-scale complete LSCF-based cells [51]. The impedance diagram is not well defined, in accordance with the superimposition of overlapping phenomena, as observed for instance in published studies concerning impedance measurements of complete anode/electrolyte/cathode cells of YSZ–Ni/YSZ/LSM [36,52], Ni–$Sm_{0.2}Ce_{0.8}O_{2-\delta}$(SDC)/SDC/LSCF-SDC/LSCF [53], Ni–$Gd_{0.1}Ce_{0.9}O_{2-\delta}$(GDC)/$Sm_{0.075}Nd_{0.075}Ce_{0.85}O_{2-\delta}$(SDC)/LSCF [54] or Ni–$BaCe_{0.8}Sm_{0.2}O_{2-\delta}$(BCS)–GDC/BCS–GDC/$Sm_{0.5}Sr_{0.5}CoO_{3-\delta}$–SDC [55]. Nevertheless the resistance observed at high frequency intercept with the real axis is in agreement with the electrolyte resistance values measured previously. The U/J curve is linear over the whole studied J range, with a slope, which represents the total resistance of the complete cell, of 0.87 Ω cm^{-2}, i.e. in good agreement with the low frequency intercept of the impedance diagram with the real axis, which is 0.91 Ω cm^{-2}. Studies concerning symmetrical electrode/electrolyte/electrode cells have concluded that there is at least two contributions due to cathode phenomena (charge transfer and mass transfer), with a total ASR that can be minimized

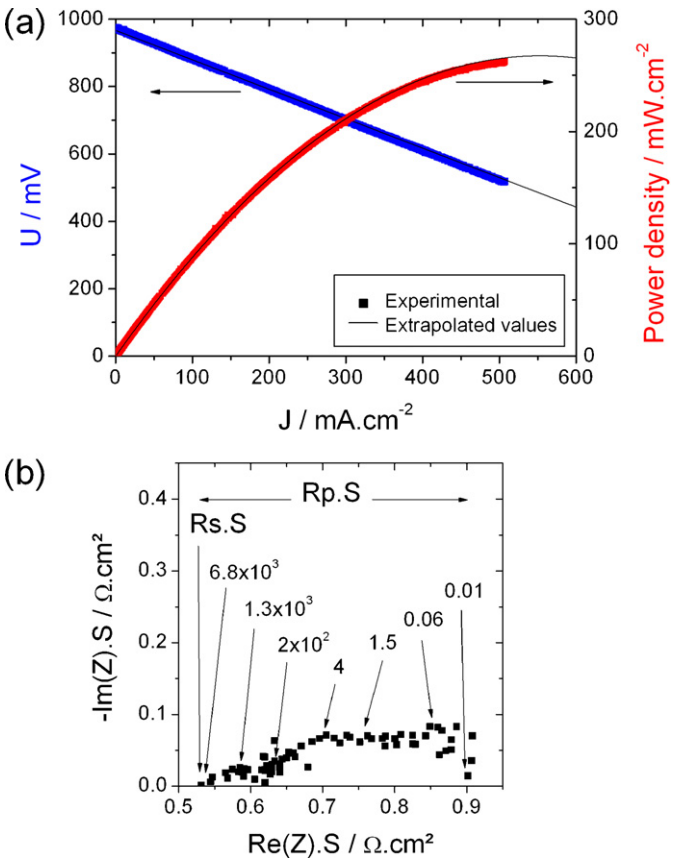

Fig. 9. Voltage and power density versus current density characteristics of the cell (■ experimental and – extrapolated) (a) and Nyquist diagram at 700 °C at OCV under wet hydrogen on the anode side and air on the cathode side (b).

to 0.07 Ω cm^{-2} and two contributions due to anode phenomena (charge transfer and mass transfer), with a total ASR that can be minimized to 0.15 Ω cm^{-2}. This suggests that the sum of the contributions of the two electrodes must reveal a total impedance diagram made of at least 4 overlapping contributions, with a difference between the high frequency and low frequency intercepts with the real axis (i.e. the total polarization resistance Rp of the cell) that cannot be smaller than 0.22 Ω cm^{-2}.

The effective Rp measured in Fig. 9b is of 0.38 Ω cm^{-2}, revealing that the total polarization of the cell is not the exact sum of the resistance of each cell component. Several authors have tried to correlate impedance measurement results obtained with complete anode/electrolyte/cathode cells with those obtained with anode/electrolyte/anode and cathode/electrolyte/cathode symmetrical cells. As it is the case in this study, in the literature, the diagram obtained for the complete cell shows the presence of at least 4 or 5 overlapping phenomena, and even with a complex mathematical treatment [34,36,47,52,56,57] it is not always possible to deconvoluate these phenomena. Therefore, it seems that all phenomena involved in the symmetrical cells are also occurring in the complete cell and that results obtained in optimizing each part of the cell separately can be used for the design of the complete cell. Nevertheless, as it is the case in the present study, the ASR measured for the total cell does not correspond simply to the sum of the ASR measured for the anode/electrolyte and electrolyte/cathode assemblies. Indeed, the reactions occurring at one electrode of the complete cell are undoubtedly influenced by the reactions occurring at the other side of the electrolyte, and the corresponding impedance response is not the same if the electrode at the opposite side of the electrolyte is the same, as it is the case in a symmetrical cell configuration, or if it is different, as it is the case in the complete cell configuration.

4. Conclusion

In the present study electrical impedance spectroscopy is used to understand the impedance diagram of the complete BIT07–Ni/BIT07/LSCF cells. The shape of this diagram has been interpreted using impedance measurements performed on BIT07–Ni/BIT07/BIT07–Ni and LSCF/BIT07/LSCF symmetrical cells.

Using electrochemical measurements, the resistance of each part of the complete cell has been minimized, and the optimization of the complete fuel cell has been achieved, allowing to reach promising total area specific resistance and power density values.

Even if the measurements are in accordance with already published results, studies performed in the present paper at OCV, are not complete enough to fully understand the electrochemical phenomena occurring in the different parts of the complete cell, especially in the anode part, and additional studies are necessary, with experiments carried out at various voltages using a three-electrode equipment.

References

[1] B.C.H. Steele, Nature 400 (1999) 619.
[2] J.R. Macdonald, Ann. Biomed. Eng. 20 (1992) 289.
[3] Q.-A. Huang, R. Hui, B. Wang, J. Zhang, Electrochim. Acta 52 (2007) 8144.
[4] V. Jayaraman, A. Magrez, M. Caldes, O. Joubert, M. Ganne, Y. Piffard, L. Brohan, Solid State Ionics 170 (2004) 17.
[5] D. Prakash, T. Delahaye, O. Joubert, M.-T. Caldes, Y. Piffard, J. Power Sources 167 (2007) 111.
[6] M. Letilly, A. Le Gal La Salle, M. Caldes, M. Marrony, O. Joubert, Fuel Cells 9 (2009) 622.
[7] M. Letilly, A. Le Gal La Salle, A. Lachgar, O. Joubert, J. Power Sources 195 (2010) 4779.
[8] Y. Tao, H. Nishino, S. Ashidate, H. Kokubo, M. Watanabe, H. Uchida, Electrochim. Acta 54 (2009) 3309.
[9] C. Torres-Garibay, D. Kovar, J. Power Sources 192 (2009) 396.
[10] S. Lee, H.S. Song, S.H. Hyun, J. Kim, J. Moon, J. Power Sources 187 (2009) 74.
[11] J. Deseure, L. Dessemond, Y. Bultel, E. Siebert, J. Eur. Ceram. Soc. 25 (2005) 2673.
[12] M. Gaudon, C. Laberty-Robert, F. Ansart, L. Dessemond, P. Stevens, J. Power Sources 133 (2004) 214.
[13] C. Torres-Garibay, D. Kovar, A. Manthiram, J. Power Sources 187 (2009) 480.
[14] M. Letilly, O. Joubert, A. Le Gal La Salle, in press.
[15] F. Tietz, Ionics 5 (1999) 129.
[16] M. Letilly, A. Le Gal La Salle, O. Joubert, Proc. of European Fuel Cell Forum (EFCF), Lucerne, Suisse, 11, 2010, 2010, p. 11.
[17] M. Letilly, M. Caldes, O. Joubert, A. Le Gal La Salle, Int. J. Hydrogen Energy, submitted for publication.
[18] E. Quarez, S. Noirault, A. Le Gal La Salle, P. Stevens, O. Joubert, J. Power Sources 195 (2010) 4923.
[19] Bio-Logic Science Instrument, Linear vs. non-linear systems in impedance measurements, http://www.bio-logic.info/potentiostat/notes/Application note 9.pdf.
[20] J. Chen, F. Liang, B. Chi, S.P. Jiang, L. Jian, J. Power Sources 194 (2009) 275.
[21] F. Boulc'h, L. Dessemond, E. Djurado, Solid State Ionics 154–155 (2002) 143.
[22] K.S. Cole, R.H. Cole, J. Chem. Phys. 9 (1941) 341–351.
[23] J.R. MacDonald, Impedance Spectroscopy Emphasizing Solid Materials and Systems, Wiley, New York, 1987.
[24] C. Brahim, A. Ringuedé, M. Cassir, M. Putkonen, L. Niinistö, Appl. Surf. Sci. 253 (2007) 3962.
[25] Y. Li, M. Liu, J. Gong, Y. Chen, Z. Tang, Z. Zhang, Mater. Sci. Eng. B 103 (2003) 108.
[26] D. Yu Wang, A.S. Nowick, J. Solid State Chem. 35 (1980) 325.
[27] S.B. Adler, Chem. Rev. 104 (2004) 4791.
[28] W.-X. Kao, M.-C. Lee, T.-N. Lin, C.-H. Wang, Y.-C. Chang, J. Power Sources 195 (2010) 2220.
[29] Y.J. Leng, S.H. Chan, K.A. Khor, S.P. Jiang, Int. J. Hydrogen Energy 29 (2004) 1025.
[30] C. Fu, K. Sun, N. Zhang, X. Chen, D. Zhou, Electrochim. Acta 52 (2007) 4589.
[31] Y. Lin, S.A. Barnett, Solid State Ionics 179 (2008) 420.
[32] P. Hjalmarsson, M. Søgaard, M. Mogensen, Solid State Ionics 180 (2009) 1395.
[33] J.-. Kim, G.-D. Kim, J.-W. Moon, Y.-I. Park, W.-H. Lee, K. Kobayashi, M. Nagai, C.-E. Kim, Solid State Ionics 143 (2001) 379.
[34] D. Ding, M. Gong, C. Xu, N. Baxter, Y. Li, J. Zondlo, K. Gerdes, X. Liu, J. Power Sources 196 (2011) 2551.
[35] S.B. Adler, Solid State Ionics 135 (2000) 603.
[36] I.M. Torres da Silva, J. Nielsen, J. Hjelm, M. Mogensen, ECS Trans. 25 (2009) 489.
[37] M. Shah, S.A. Barnett, Solid State Ionics 179 (2008) 2059.
[38] Z. Lu, J. Hardy, J. Templeton, J. Stevenson, J. Power Sources 196 (2011) 39.

[39] H. Xiong, B.-K. Lai, A.C. Johnson, S. Ramanathan, J. Power Sources 193 (2009) 589.
[40] F. Qiang, K. Sun, N. Zhang, X. Zhu, S. Le, D. Zhou, J. Power Sources 168 (2007) 338.
[41] W.G. Wang, M. Mogensen, Solid State Ionics 176 (2005) 457.
[42] F.S. Baumann, J. Fleig, H.-U. Habermeier, J. Maier, Solid State Ionics 177 (2006) 1071.
[43] V. Dusastre, J.A. Kilner, Solid State Ionics 126 (1999) 163.
[44] D.E. Vladikova, Z.B. Stoynov, A. Barbucci, M. Viviani, P. Carpanese, J.A. Kilner, S.J. Skinner, R. Rudkin, Electrochim. Acta 53 (2008) 7491.
[45] J.-W. Lee, Z. Liu, L. Yang, H. Abernathy, S.-H. Choi, H.-E. Kim, M. Liu, J. Power Sources 190 (2009) 307.
[46] Y.-M. Kim, S.-W. Baek, J. Bae, Y.-S. Yoo, Solid State Ionics 192 (2010) 595.
[47] R. Barfod, M. Mogensen, T. Klemenso, A. Hagen, Y.L. Liu, P. Vang Hendriksen, J. Electrochem. Soc. 154 (2007) B371–B378.
[48] S.W. Baek, J. Bae, Int. J. Hydrogen Energy 36 (2011) 689.
[49] M.C. Verbraeken, B.A. Boukamp, D.H.A. Blank, P. Holtappels, U. Vogt, in: S.C. Singhal, J. Mizusaki (Eds.), Electrochemical Society Proceedings 07, 2 volume set, Solid Oxide Fuel Cell (SOFC IX), 2005, pp. 1218–1225, ISBN:1-56677-465-9.
[50] Z. Jiao, N. Takagi, N. Shikazono, N. Kasagi, J. Power Sources 196 (2011) 1019.
[51] T.-J. Huang, X.-D. Shen, C.-L. Chou, J. Power Sources 187 (2009) 348.
[52] H. Schichlein, A.C. Müller, M. Voigts, A. Krüger, E. Ivers-Tiffée, J. Appl. Electrochem. 32 (2002) 875.
[53] S.-F. Wang, Y.-R. Wang, C.-T. Yeh, Y.-F. Hsu, S.-D. Chyou, W.-T. Lee, J. Power Sources 196 (2011) 977.
[54] J.S. Ahn, S. Omar, H. Yoon, J.C. Nino, E.D. Wachsman, J. Power Sources 195 (2010) 2131.
[55] W. Sun, Y. Jiang, Y. Wang, S. Fang, Z. Zhu, W. Liu, J. Power Sources 196 (2011) 62.
[56] S. McIntosh, J.M. Vohs, R.J. Gorte, J. Electrochem. Soc. 150 (2003) A1305.
[57] A. Leonide, V. Sonn, A. Weber, E. Ivers-Tiffée, J. Electrochem. Soc. 155 (2008) B36.